2009

A Study of Microstructures and Tensile Properties of Two Fe-Mn-Al-Si-C Alloys

B. Bhattacharya
Tata Steel Limited, Jamshedpur, India

A. Sharma
Indian Institute of Technology, Kanpur, India

Sujoy Hazra
University of Wollongong, ssh755@uow.edu.au

R. Ray
Indian Institute of Technology, Kanpur, India

A Study of Microstructures and Tensile Properties of Two Fe-Mn-Al-Si-C Alloys

B. BHATTACHARYA, A.S. SHARMA, S.S. HAZRA, and R.K. RAY

Two high-manganese steel compositions were prepared (low-carbon steel (LC): 0.05C-26.3Mn-4.88Si-4.13Al-Fe, and high-carbon steel (HC): 0.52C-29.8Mn-2.96Si-2.73Al-Fe). These were homogenized, hot rolled, heat treated, and finally subjected to tensile testing and other characterizations. The LC steel, with a duplex microstructure containing body-centered-cubic (bcc) and face-centered-cubic (fcc) phases, exhibited extremely poor room-temperature ductility. On the other hand, the HC steel, with a single-phase austenitic structure, showed a good tensile property due to twin-induced plasticity (TWIP) effect, with total tensile elongation as high as 56 pct. Structural analysis of steel LC was carried out and it was found that the bcc phase of steel LC was actually an ordered DO_3 phase, which was identified as the principal reason of poor ductility of steel LC.

DOI: 10.1007/s11661-009-9797-1

I. INTRODUCTION

THE ever-increasing demand for advanced materials in the automobile sector, in terms of higher strength-to-weight ratio and adequate formability, has led to the development of various advanced high-strength steels. Among these steel grades, high-manganese austenitic steels are considered potential candidates for the manufacturing of automobile components that require superior crash resistance. The most important characteristics of this family of steels are stable austenitic (face-centered-cubic (fcc)) structure and twinning mode of deformation. This results in excellent work-hardening property, leading to a combination of high ductility and high strength.[1,2]

The stability of austenite phase depends on alloying. Various studies have been carried out with many such steel compositions.[1–7] A higher manganese content (more than 20 pct) is responsible for twin-induced plasticity (TWIP) effect, while a lower manganese content, around 15 pct, leads to transformation-induced plasticity (TRIP) effect.[2] The phase stability of these steels is yet to be understood completely, though significant research efforts have also been applied in that area.[8–10] The present work was undertaken with an objective of studying the development of TWIP effect in two high-Mn steels, especially the low-carbon variety, and correlating this phenomenon with their mechanical properties.

B. BHATTACHARYA, Researcher, is with the R&D Division, Tata Steel Limited, Jamshedpur, India. Contact e-mail: basudev@tatasteel.com A.S. SHARMA, formerly Research Assistant, R&D Division, Tata Steel Limited, is Doctoral Student, Indian Institute of Technology, Kanpur, India. S.S. HAZRA, formerly Researcher, R&D Division, Tata Steel Limited, is Doctoral Student on Study Leave, University of Wollongong, Wollongong, Australia. R.K. RAY, formerly Professor of Materials and Metallurgical Engineering, Indian Institute of Technology, Kanpur, is Visiting Scientist, R&D Division, Tata Steel Limited, Jamshedpur, India.

Manuscript submitted August 9, 2008.
Article published online February 20, 2009

II. EXPERIMENTAL

Two high-manganese steel compositions, namely, low-carbon steel (LC) and high-carbon steel (HC), were selected for this work. The chemical compositions of the two steels are shown in Table I. The principal difference between the two compositions was that steel LC had a low carbon composition and steel HC was basically a medium-carbon steel, both heavily alloyed with manganese, aluminum, and silicon.

The steels were prepared by melting steel scrap, along with other constituents such as ferromanganese, ferrosilicon, and aluminum blocks, in an induction furnace, and subsequently cast into 25 kg ingots of approximate dimensions 120 × 120 × 300 mm. Wire-cut electro discharge machining (EDM) was used for the cutting of ingots into small pieces of samples in order to avoid the difficulty that could arise due to work-hardening behavior of austenitic steels. The ingots were cut into smaller pieces for further processing. The final dimensions of the cast steel pieces were 40 × 60 × 120 mm, which were subsequently soaked in a laboratory furnace at 1120 °C for 2 hours and then hot rolled to a thickness of 5.5 mm in five passes using a two-high laboratory rolling mill having 300-mm diameter work rolls. The constant rolling speed was 80 m/min, and the finish rolling temperature was maintained at approximately 870 °C (±3 °C). The temperature measurement utilized a digital optical pyrometer, which was calibrated using a few dummy samples before the start of actual experiment, with thermocouples welded to those samples. The rolling draft schedule for the five passes was 40 → 24 → 16 → 9 → 6.5 → 5.5 mm. Apart from hot rolling, a set of homogenization experiments was carried out with smaller samples (10 × 8 × 5 mm) cut out from the cast ingot. The hot-rolled steels were further isothermally heat treated in a laboratory muffle furnace for 2 hours at two different temperatures, 800 °C and 1050 °C. Specimens for microstructure study were

prepared from the longitudinal surface for the cast samples, homogenized samples, hot-rolled samples, and also for the samples which were further heat treated. Tensile specimens were prepared according to ASTM E8 specification from the hot-rolled samples and also from the samples heat treated at 1050 °C. Due to small width of the hot-rolled samples, all tensile samples were prepared along the rolling direction. Tensile tests were carried out in an Instron universal testing machine, maintaining a crosshead velocity of 5 mm/min before yield point and 40 mm/min after yield point. All microstructure specimens were chemically etched, using 2 or 5 pct nital solution, as applicable. The electron back scatter diffraction (EBSD) samples were prepared by polishing the longitudinal surfaces, while the X-ray diffraction (XRD) samples were prepared by polishing the midthickness surfaces parallel to rolling plane. Optical micrographs were taken in a Zeiss microscope (Zeiss, Vorpommern, Germany). The scanning electron microscope (SEM) micrographs were taken in a Zeiss (Zeiss, Vorpommern, Germany) field emission scanning electron microscope (FE-SEM), with energy dispersive spectrum (EDS) and EBSD attachment. All XRD runs were taken in a fully automatic Panalytical (PANalytical B.V., Almelo, The Netherlands) X-ray diffractometer, using Cu K_α radiation.

Table I. Chemical Composition of Experimental Alloys (Weight Percent)

Steel Compositions	C	Mn	Si	Al
LC	0.05	26.3	4.88	4.13
HC	0.52	29.8	2.96	2.73

III. RESULTS AND DISCUSSION

A. *Microstructure of Homogenized and Hot-Rolled Steels*

Cast and homogenized microstructures of steels LC and HC are shown in Figure 1. The microstructure of LC clearly depicts two phases, both before and after homogenization heat treatment at 1100 °C for 2 hours (Figures 1(a) and (b)). The cast microstructure of HC shows typical dendritic solidification structure (Figure 1(c)). Single-phase austenite microstructure was developed after homogenization (Figure 1(d)). The phase mapping picture obtained from the orientation imaging microscopy of steel LC is shown in Figure 2, which reveals that the matrix phase has body-centered-cubic (bcc) crystal structure and the second phase has fcc structure. It may be concluded immediately that the

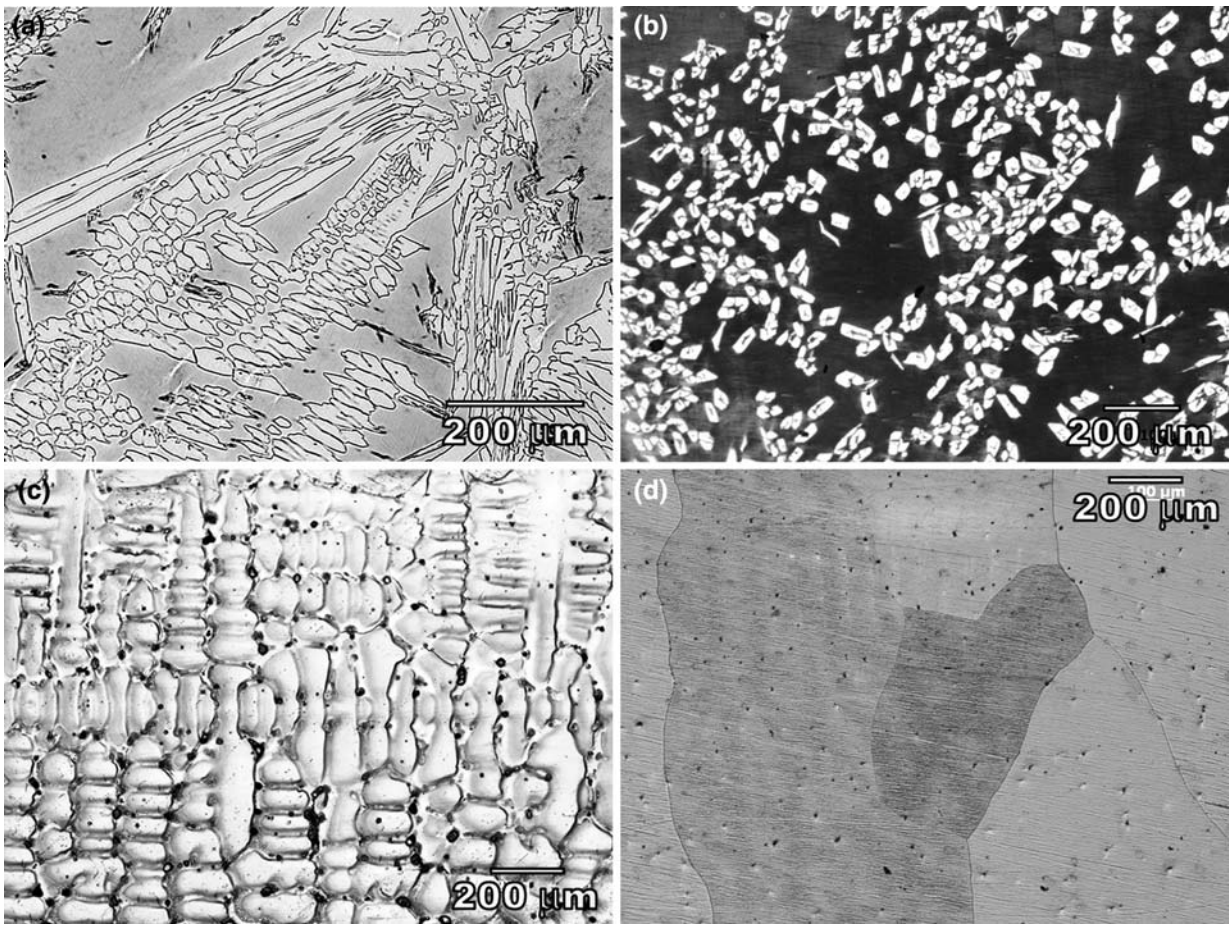

Fig. 1—Cast and homogenized microstructures of two steels: (*a*) cast LC, (*b*) homogenized LC, (*c*) cast HC, and (*d*) homogenized HC.

microstructure of steel LC actually features dispersed austenite phase within a ferrite matrix. In case of steel HC, the single-phase microstructure was austenite, which

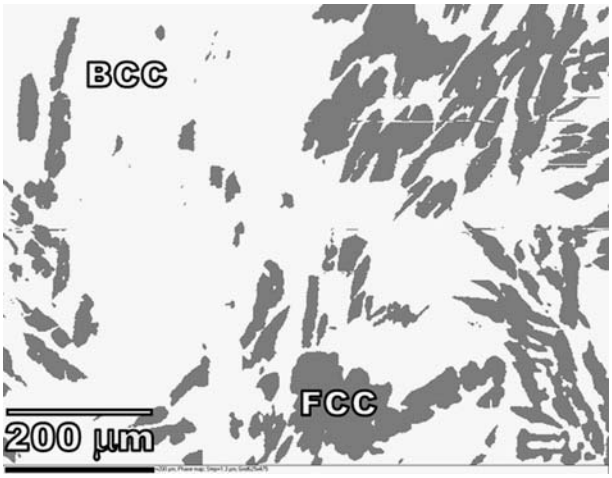

Fig. 2—Phase mapping picture of cast LC (orientation imaging).

was confirmed through various other characterizations discussed subsequently in this article. The EDS spectra analysis of cast LC reveals the elemental distribution, which is shown in Figure 3. It is important to note that manganese concentration in austenite phase is more than that in ferrite phase. That means that manganese preferably partitions into austenite phase, while aluminum and silicon exhibit somewhat opposite behavior.

The hot-rolled microstructures are shown in Figure 4. Two photomicrographs (Figures 4(a) and (b)) indicate that there is a distinct difference in the distribution and morphology of austenite phase at two locations in steel LC after hot rolling. The microstructures of hot-rolled LC do not reveal the presence of twin bands in austenite phase, if any. On the other hand, the expected twin bands were clearly observed in the microstructure of steel HC (Figure 4(c)). No significant through-thickness variation in microstructure was noticed in steel HC, and a uniform fine grain structure was developed throughout the thickness. The structural heterogeneity of sample LC is possibly a result of combination of two effects, (a) differential through-thickness rolling strain and (b)

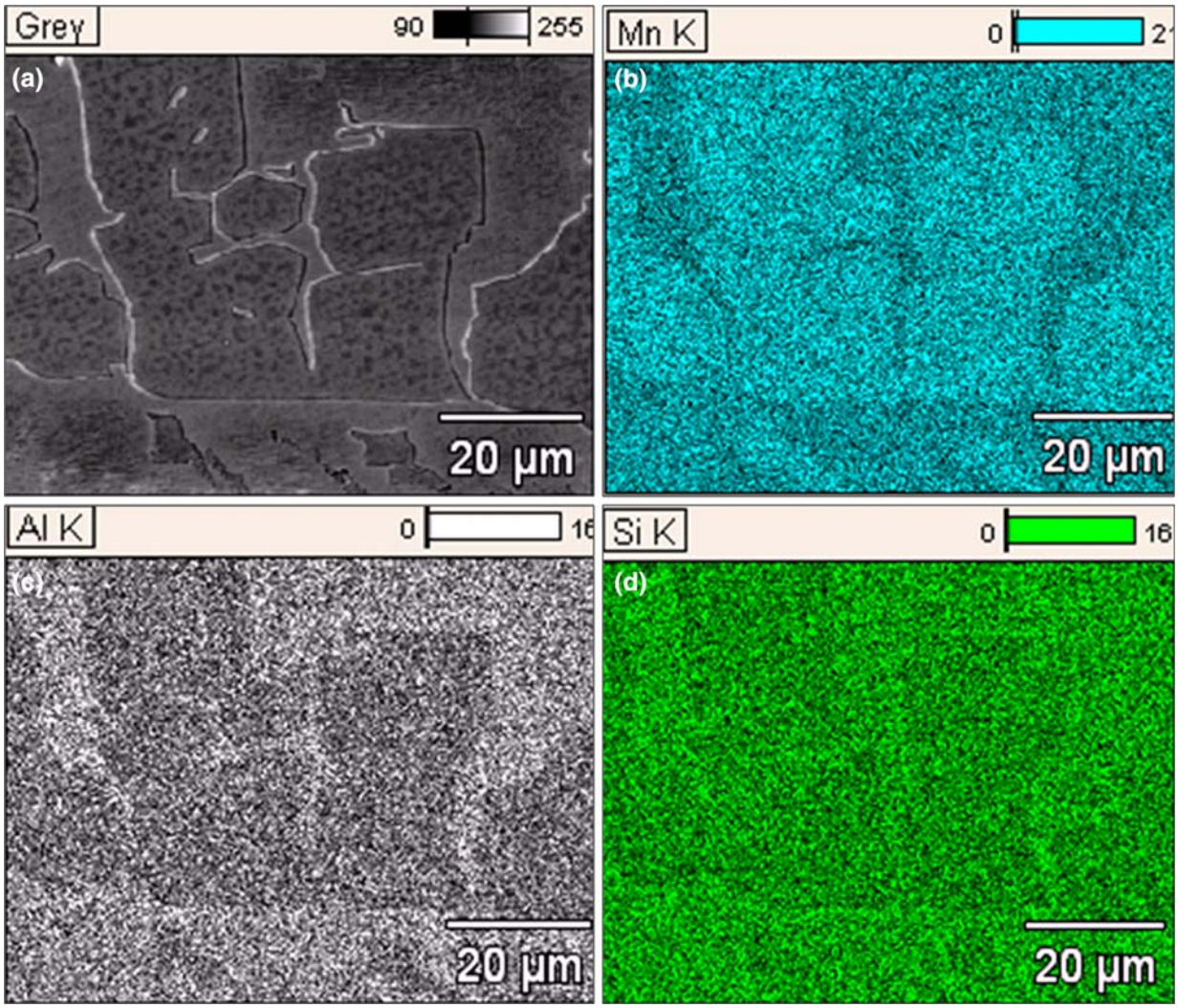

Fig. 3—Elemental mapping of steel LC (cast). Gray scale picture, Mn—mapping, Al—mapping, and Si—mapping.

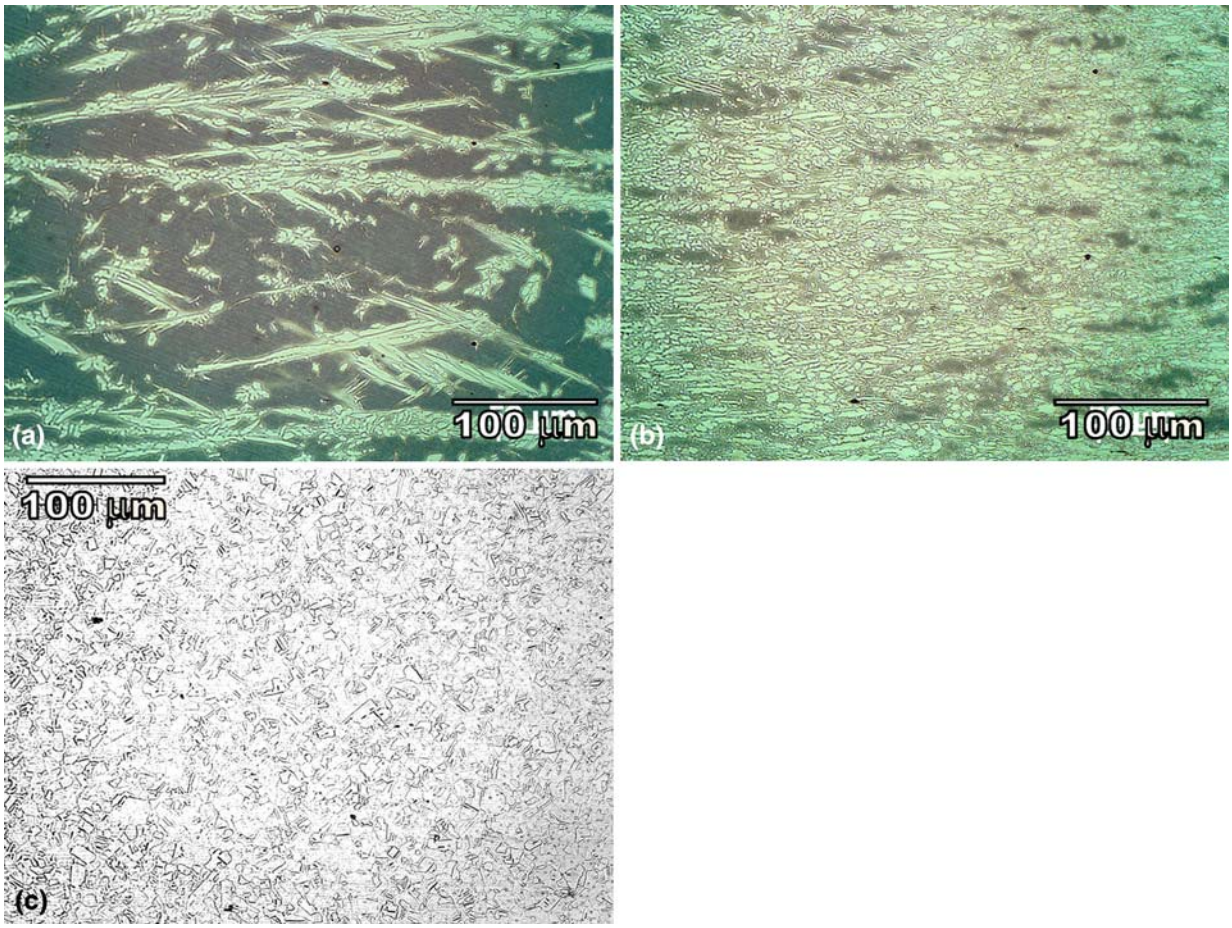

Fig. 4—Hot-rolled microstructures of two steels. (*a*) LC at midthickness, (*b*) LC close to surface, and (*c*) HC at midthickness.

precipitation of austenite, leading to increase in austenite volume. In case of steel HC, only differential rolling strain was active. As a result, there was no significant difference in microstructures at surface and middle after recrystallization. But in case of steel LC the additional factor of austenite precipitation (which is evident from Figure 6(a), after heat treatment of hot-rolled LC) came into the picture and most probably this effect was more prominent due to larger strain close to the surface, which ultimately created a totally different microstructure. The frequency percentages of coincidence boundaries (CSL) in both hot-rolled steels, LC and HC, as obtained through orientation imaging technique, are shown in Figure 5. It was observed that the population of Σ3 boundaries in fcc phase of hot-rolled steel LC was near 3 pct, along with insignificant presence of few other Σ boundaries in bcc and fcc phases. This indicates that twin boundaries actually developed in fcc phase, though it was not clearly understood from the optical micrographs (Figures 4(a) and (b)). On the other hand, in steel HC much stronger existence of Σ3 boundaries and negligible presence of other boundaries (Figure 5) clearly indicate the formation of a twinned microstructure.

The hot-rolled steels, as mentioned previously, were heat treated for 2 hours at two different temperatures, 800 °C and 1050 °C. The microstructures of these heat-treated steels are shown in Figure 6. After heat

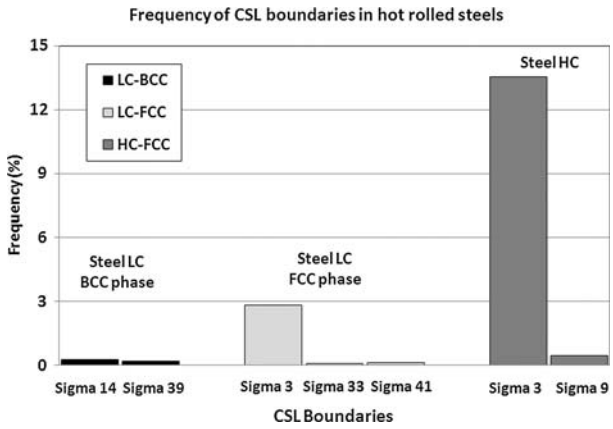

Fig. 5—Population (in frequency percentage) of CSL boundaries in hot-rolled steels LC and HC.

treatment, steel LC showed a completely different picture. At 800 °C, a fine network of austenite phase was developed (Figure 6(a)). It is evident that the austenite volume fraction significantly increased after heat treatment. The microstructure further changed after heat treatment at 1050 °C (Figure 6(b)) and discrete islands of austenite phase could be observed

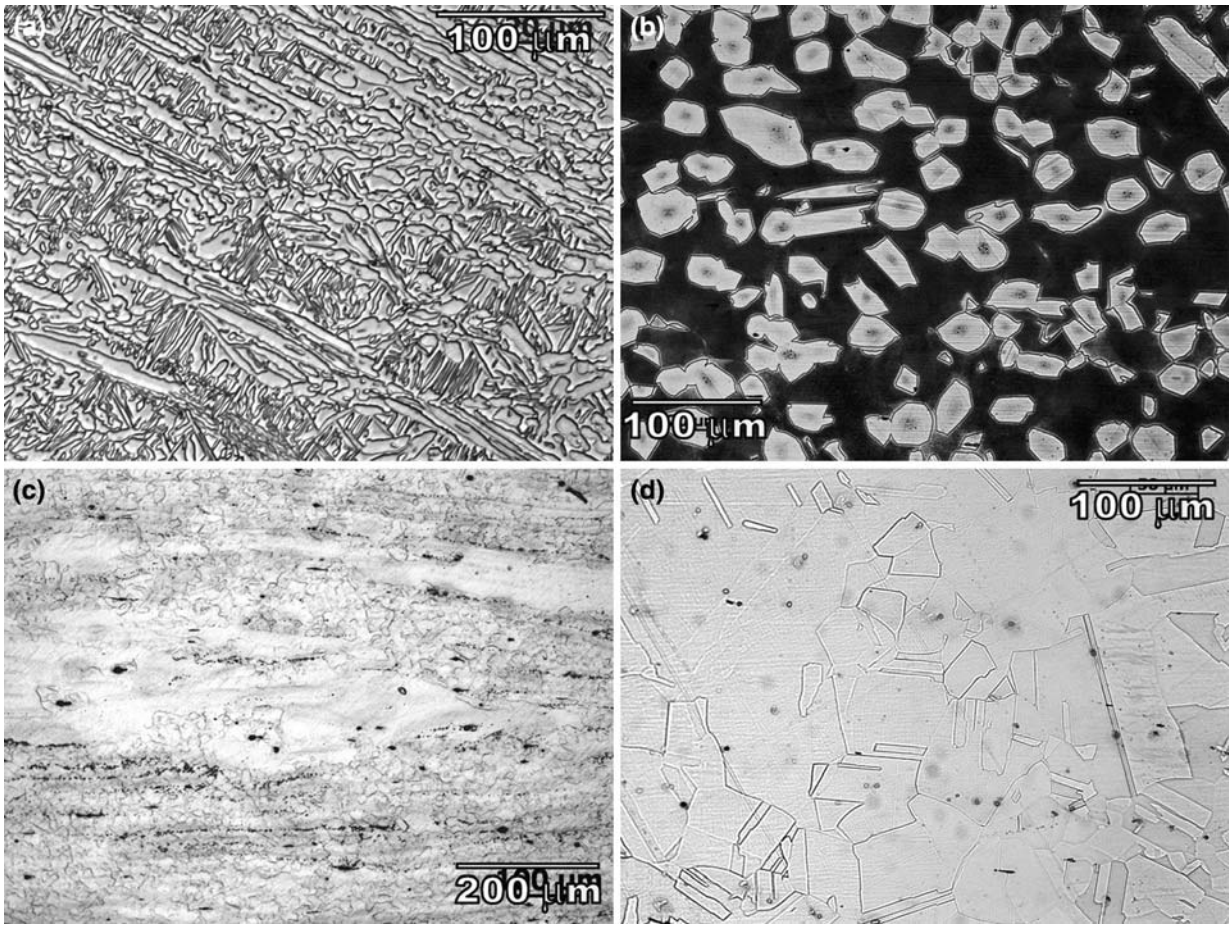

Fig. 6—Microstructures of two steels after two post-hot-rolling heat treatments: (*a*) steel LC, hot rolled + heat treated at 800 °C for 2 h; (*b*) steel LC, hot rolled + heat treated at 1050 °C for 2 h; (*c*) steel HC, hot rolled + heat treated at 800 °C for 2 h; (*d*) steel HC, hot rolled + heat treated at 1050 °C for 2 h.

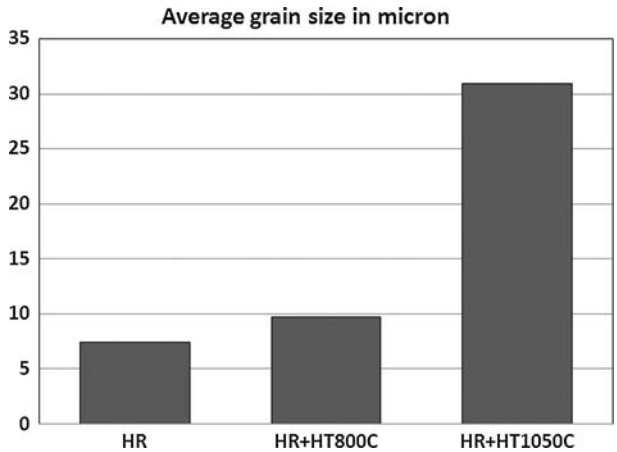

Fig. 7—Average grain sizes of steel HC in different conditions.

within the matrix of ferrite phase. A careful look at this photomicrograph would also reveal the twin bands in the austenite phase.

On the other hand, there was not much change in the basic nature of microstructure for steel HC after the heat treatments. Twinned microstructure, which is a characteristic of austenite phase, could be observed clearly in these photographs (Figures 6(c) and (d)). A number of deformation bands and partially recrystallized areas could also be seen in the specimen that was heat treated at 800 °C (Figure 6(c)). The specimen that was heat treated at 1050 °C featured twinned and fully recrystallized microstructure (Figure 6(d)). A quick comparison between Figures 4(c) and 6(d) readily indicates how much the grain size increased after the heat treatment. The comparison of average grain sizes of steel HC in three different conditions, hot rolled, heat treated at 800 °C, and heat treated at 1050 °C, is shown in Figure 7.

B. *Tensile Properties*

The tensile testing data for the two steels in two different conditions are shown in Table II. Tensile tests showed that steel LC was a highly brittle material. Both the hot-rolled steel, as well as hot-rolled + heat-treated steel failed completely under tensile loading. On the other hand, steel HC showed a good blend of strength and ductility. The engineering stress-strain diagrams of steel HC in two conditions are shown in Figure 8. The ultimate tensile strength (UTS) of hot-rolled specimen

Table II. Tensile Test Data for the Two Steels

Steels	LC		HC	
Condition	hot rolled	hot rolled + heat treated (1050 °C for 2 h)	hot rolled	hot rolled + heat treated (1050 °C for 2 h)
Yield strength (MPa)	—	—	599	350
Ultimate tensile strength (MPa)	—	—	801	726
Total elongation (pct)	0	0	33 pct	56 pct
Yield ratio YS/UTS	—	—	0.748	0.482

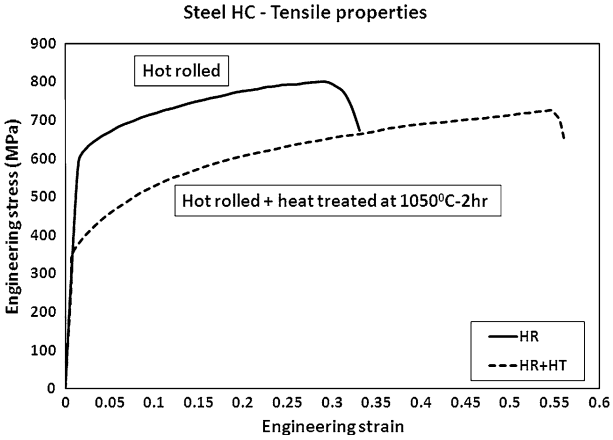

Fig. 8—Engineering stress-strain diagrams of steel HC in two conditions: hot rolled (HR) and hot rolled + heat treated at 1050 °C for 2 h (HR + HT).

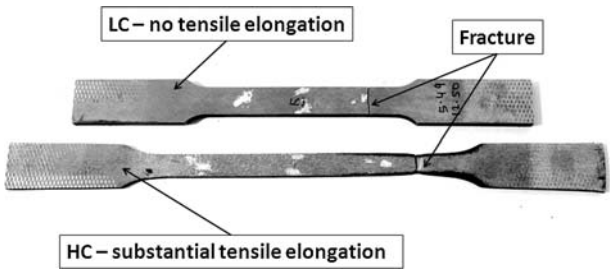

Fig. 9—Tensile specimens of two steels, hot rolled + heat treated at 1050 °C for 2 h.

was 801 MPa and the total elongation was 33 pct. After heat treatment (at 1050 °C for 2 hours), strength dropped to 726 MPa but the elongation increased to 56 pct. The yield strength (YS) value dropped by about 40 pct after heat treatment. Grain size definitely had a role to play, which can be understood readily by simultaneously considering Figure 7 and Table II. The fractured specimens of both steels, in hot-rolled + heat-treated condition are shown in Figure 9. The shapes of the specimens and the locations of fracture clearly indicate the difference in ductility of these two steels.

Microstructures of steel HC were examined on the longitudinal plane of tensile specimens, at spots close to the locations of fractures, both for hot-rolled steel and hot-rolled + heat-treated (1050 °C) steel. Both specimens underwent extensive twinning deformation during tensile testing. Optical micrographs of both specimens (Figures 10(a) and (b)), along with one SEM micrograph taken at higher magnification (Figure 10(c)), depict how numerous deformation twins and shear bands formed in the hot-rolled and heat-treated steel HC during tensile deformation. Another important point may be noted that the development of deformation twins and shear bands was much more prominent in the sample that was heat treated after hot rolling (Figures 10(b) and (c)). These bands in hot-rolled + heat-treated specimen appear to be much larger in size. Also the crossing over between these bands is also very prominent.

The TWIP effect depends on the extent of twin formation. The density of twin boundaries increases upon straining. As per Allain *et al.*,[11] the twin boundaries as well as grain boundaries are strong obstacles to twins. Also, during a deformation process both mechanical twinning and dislocation gliding enter in competition and closely interact in each grain. The stoppage of twins at the grain boundaries has also been discussed by Cornette *et al.*[12] This indicates that less availability of grain boundary would lead to more effective twin formation and stronger TWIP effect. A comparison between Figures 10(a) and (b) clearly indicates that twinning is more extensive in large size grains (Figure 10(b)). From this observation, it may be concluded that TWIP is much more effective in the specimen with larger grains size. Ueji *et al.*,[13] in their experiment with ultrafine-grain TWIP steels, also found that the total elongation increased with grain size under the same condition of testing, such as temperature, strain rate, *etc.* This is quite important from the point of view of optimization of industrial processing; the mechanical property can be controlled by developing suitable grain size.

The fracture surfaces of the two steels are shown in Figures 11 and 12. The picture of hot-rolled steel LC (Figure 11(a)) clearly shows transgranular nature of fracture. The transgranular nature of fracture was unchanged even after heat treatment (Figure 11(b)). This observation is in contrast with the results reported by Grässel *et al.*[2] In their case, a Fe-0.03C-26.5Mn-3.0Si-2.8Al steel exhibited excellent combination of strength and ductility, while in the present case a composition with little higher carbon, aluminum and silicon (0.052 pct C, 4.13 pct Al, 4.88 pct Si), completely failed under tension, practically at zero elongation.

Steel HC performed quite satisfactorily during tensile test. Figure 12(a) shows the fracture surface of the hot-rolled steel HC, which clearly indicates ductile behavior.

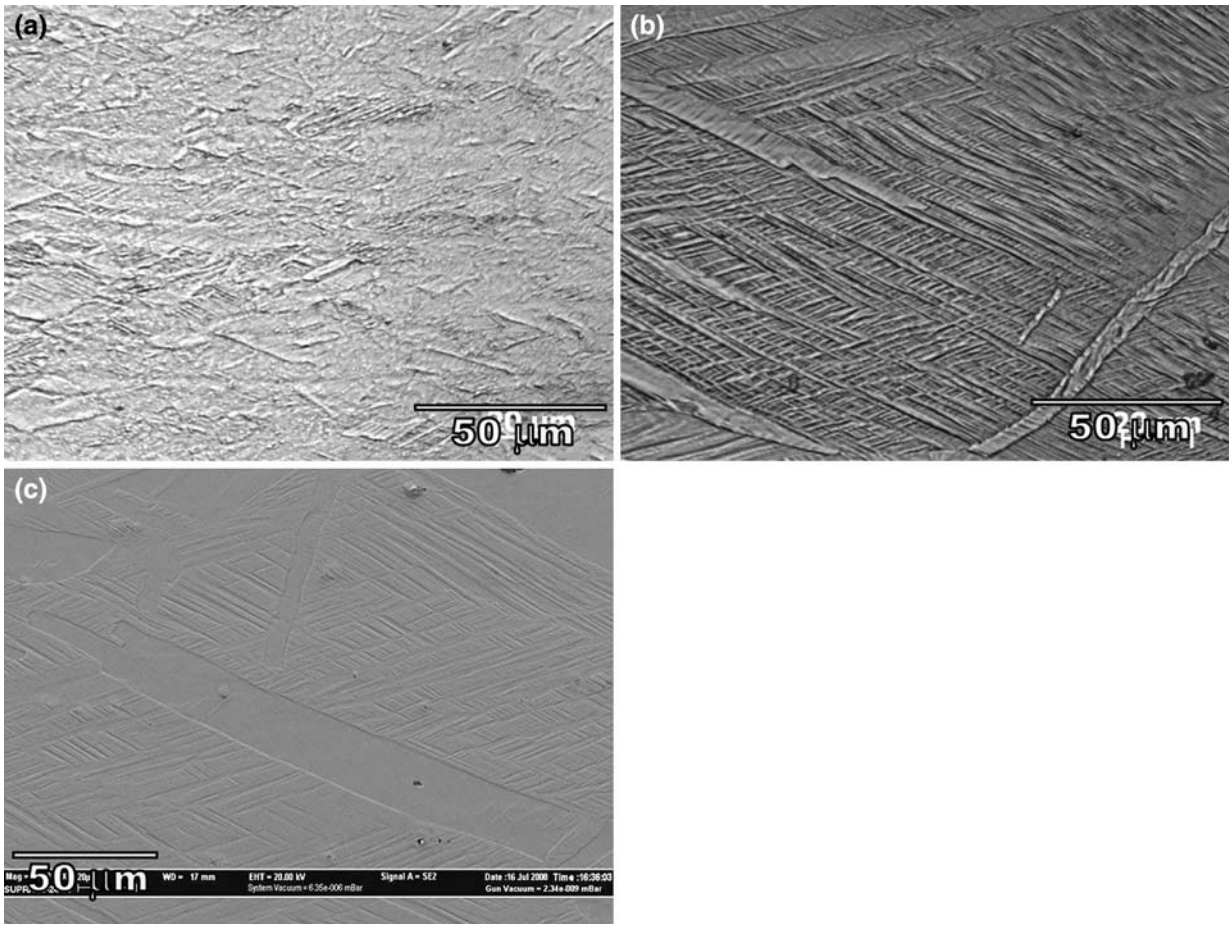

Fig. 10—Micrographs of tensile specimen of steel HC (hot rolled + heat treated at 1150 °C) after tensile deformation: (*a*) hot rolled; (*b*) hot rolled + heat treated at 1150 °C for 2 h; and (*c*) hot rolled + heat treated, SEM picture.

The fracture surface of hot-rolled + heat-treated steel HC, shown in Figure 12(b) at a high magnification, also features typical characteristics of ductile fracture.

C. *Brittleness of Steel LC*

The steel consisted of two distinct phases, one was fcc and the other was bcc, which is evident from the orientation imaging data (Figure 2). The typical transgranular nature of fracture points to the fact that the matrix of this steel was inherently brittle. The austenite phase as observed in steel HC, was highly ductile. Therefore, in order to understand the reason of brittleness of steel LC at this stage, the bcc phase of steel LC requires more attention. Two SEM photomicrographs of steel LC are shown in Figure 13 at two different conditions.

In the SEM micrograph of cast LC grade (Figure 13(a)) the bcc matrix appears to have a peculiar matrix morphology, which was not quite clear in the optical photomicrographs. The same feature of bcc phase was maintained even after the entire processing: homogenization, hot rolling, and annealing at 1050 °C for 2 hours. However, the appearance of fcc phase changed radically after the processing and well-delineated islands of austenite phase could be observed at the end (Figure 13(b)). Even the twin bands were clearly visible in the austenite islands. The morphology and the unexpected brittleness of bcc phase suggest that this is possibly not a simple ferrite phase. In order to characterize this bcc phase, extensive XRD study was conducted.

1. *XRD results*

The XRD profile of cast LC grade is shown in Figure 14. All XRD peaks were not present in this profile due to strong solidification texture effect. Some of the peaks were very weak. However, it was possible to index the available peaks and make an estimation of the phases that were present in the material. The XRD profile clearly indicated the coexistence of fcc and bcc phases in steel LC. The indexed peaks and their relative intensities (I/I_{max}) are summarized in Table III.

It is interesting to note that there are two extra peaks reflected from bcc phase, which have been indexed as (113) and (226) peaks from DO_3 phase. The DO_3 is also a bcc phase, but it has an ordered superlattice structure consisting of atoms of two different elements in a ratio of 3:1 (Figure 15).

In the next stage XRD study was carried out with both steel grades at different conditions. The XRD profiles of hot-rolled and heat-treated steels, LC and

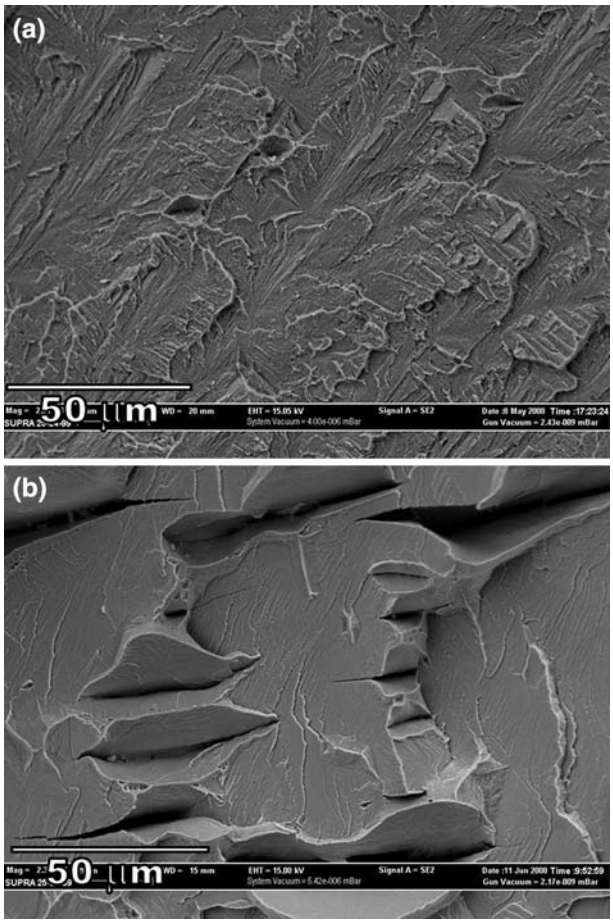

Fig. 11—Fracture surface of steel LC (*a*) hot rolled and (*b*) hot rolled + heat treated at 1050 °C for 2 h.

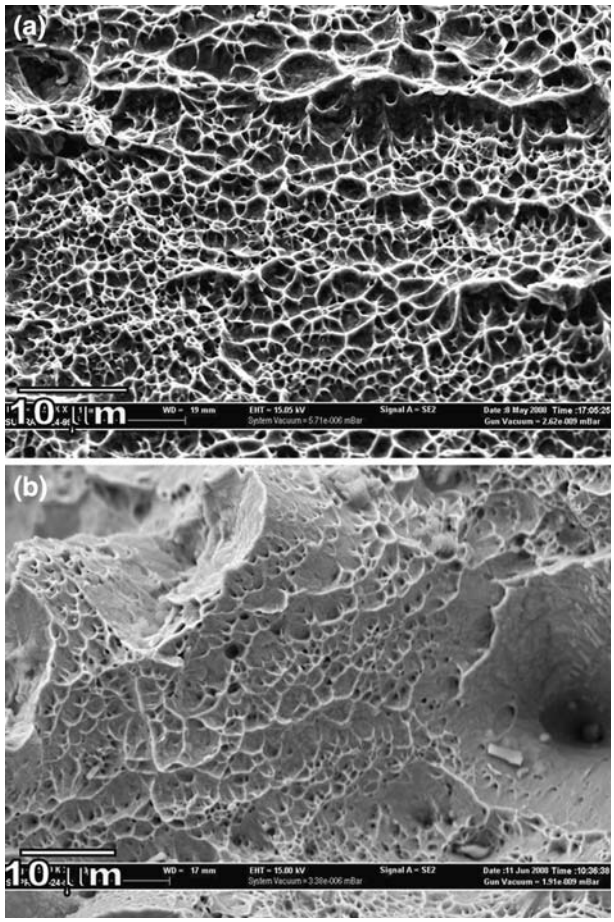

Fig. 12—Fracture surface of steel HC (*a*) hot rolled and (*b*) hot rolled + heat treated at 1050 °C for 2 h.

HC, are shown in Figures 16(a) and (b), respectively. All XRD scans were carried out on the midthickness planes of all specimens parallel to rolling plane. The indexing of all XRD profiles are summarized in Tables IV(a) and (b), respectively, for the two steels LC and HC.

It may be noticed immediately that the XRD profiles of steel LC show a combination of different crystal structures, while XRD profiles of steel HC (Figure 16(b)) indicate a single-phase fcc structure, which is expected for fully austenitic steel.

The XRD profiles of steel LC (Figure 16(a) and Table IV(a)) exhibit quite a few features, which may be listed as follows:

(a) presence of two main phases, ferrite (bcc) and austenite (fcc);
(b) presence of prominent superlattice peaks from DO_3 phase (ordered bcc);
(c) (200) peak of DO_3 phase is the strongest reflection of that phase;
(d) reflection from bcc phase is the strongest in all conditions because of the major volume fraction of bcc phase;
(e) strengths of fcc reflections are highest in the specimen that was heat treated at 800 °C and moderate in the specimen that was heat treated at 1050 °C, fcc-220 being a fairly strong reflection;
(f) the bcc-110 peak, which is extremely weak in the hot-rolled specimen and completely absent in the specimen heat treated at 1050 °C, appears to be the strongest peak in the specimen that was heat treated at 800 °C;
(g) the strengthening of bcc-200, bcc-110, and bcc-112 peaks at three different conditions gives some indirect indication about the changes of grain orientation; and
(h) the fcc phase reflections became stronger after heat treatment, which is corroborated by Figure 6(a), giving an indication of increase in volume fraction of austenite phase with heat treatment.

In the XRD profiles of steel HC (Figure 16(b) and Table IV(b)), the only significant change that may be noticed is the sharpening of (111) peak with annealing, with further enhancing of that peak in the sample that was heat treated at a higher temperature, 1050 °C.

2. *Ordering of DO_3 phase in steel LC*

Both aluminum and silicon form ordered bcc phases (α_1) with Fe, namely, Fe_3Al and Fe_3Si with DO_3 superlattice structure (Pearson symbol *cF*16).[14]

Considering simultaneous presence of both these elements in substantial quantities, it is quite likely that the DO_3 phase in steel LC consists of both Fe_3Al and Fe_3Si.

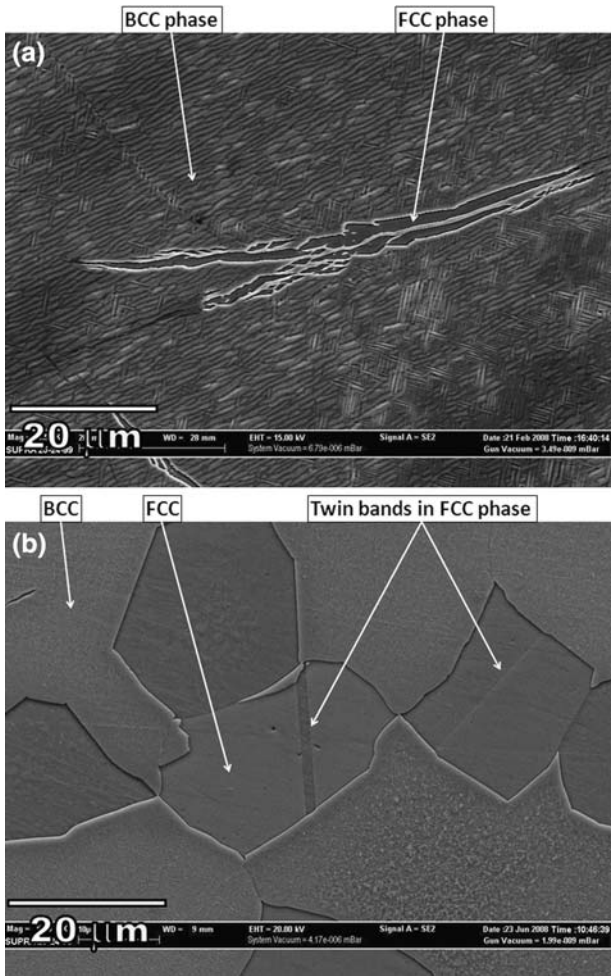

Fig. 13—SEM photomicrographs of steel LC (*a*) cast steel and (*b*) hot rolled and heat treated at 1050 °C for 2 h.

An attempt was made to measure the order parameter of DO_3 phase of steel LC, separately considering both the intermetallic compounds Fe_3Al and Fe_3Si. For this purpose, a set of two XRD reflections, a superlattice peak, and the corresponding fundamental peak from two parallel planes were selected. The reason for such selection is that the relative intensities of reflections from these two parallel planes would be proportionally influenced by crystallographic texture; as a result, their integrated intensity ratio would remain unchanged irrespective of texture. One such set was identified as DO_3-200 and bcc-200 peaks. The integrated areas under these peaks were measured and the order parameter S was calculated as per the following relationship[15]

$$S^2 = \left(\frac{I_s}{I_f}\right) \cdot 16 \cdot \left\{\frac{(X_{Fe} f_{Fe} + Xf)^2}{(f_{Fe} - f)^2}\right\} \cdot \left\{\frac{(L_p)_{fu}}{(L_p)_{su}}\right\} \cdot \left\{\frac{(e^{-2M})_{fu}}{(e^{-2M})_{su}}\right\} \quad [1]$$

where I = integrated intensity of XRD peaks; X_{Fe} = atomic fraction of Fe; X = atomic fraction of either Al or Si; f_{Fe} = atomic scattering factor of Fe; f = atomic scattering factor of either Al or Si; L_p = Lorentz polarization factor; e^{-2M} = Debye–Waller temperature factor; and subscripts *su* and *fu* refer to the superlattice and fundamental peaks, respectively.

For the purpose of S parameter calculation, separately considering Fe_3Al and Fe_3Si, integrated intensity values were directly measured from the XRD profiles, atomic fractions of Fe, Al and Si were obtained from the spot EDS analysis data measured specifically on the bcc phase, as shown in Table V, atomic scattering factors and Lorentz polarization factors were obtained directly from standard charts available in the literature.[16] The Debye–Waller temperature factor has little importance, since all measurements were carried out at room temperature. The calculated S parameters for steel LC in three conditions are shown in Figure 17. In the hot-rolled condition, the order parameter was

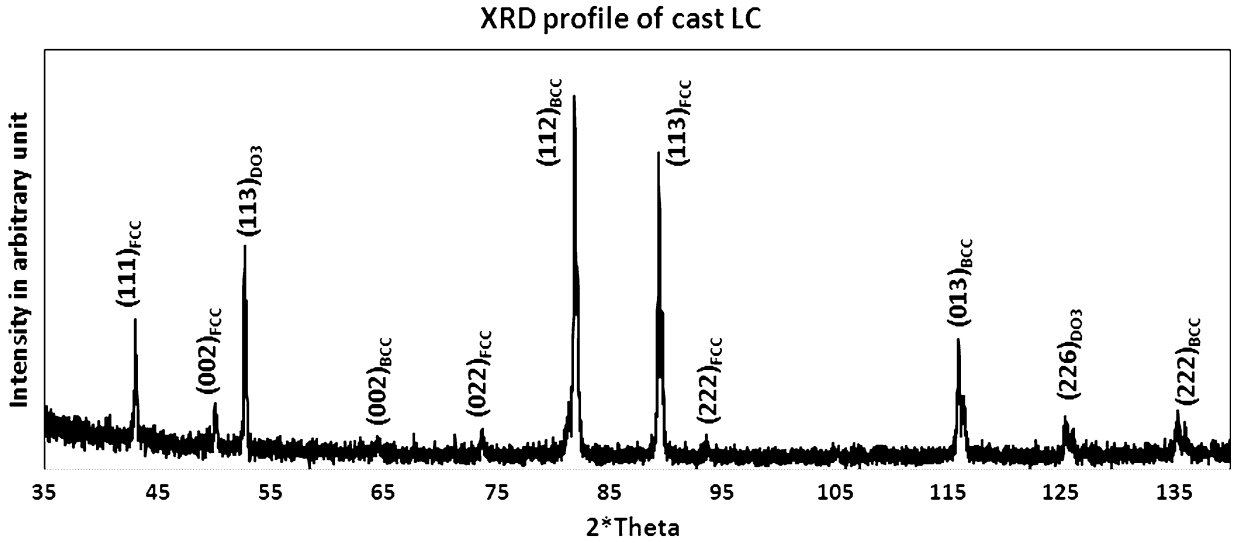

Fig. 14—XRD profile of cast LC.

Table III. Summary of XRD Peaks Obtained from Cast LC Material

Phases	Reflecting Planes	Peak Positions	d Spacing (Å)	I/I_{max} (Pct)	Remark
Fcc	111	~43 deg	2.10037	35.7	moderately strong
	002	~50 deg	1.81834	10.2	weak
	022	~73.5 deg	1.28343	3	very weak
	113	~89.5 deg	1.09528	80.6	very strong
	222	~94.5 deg	1.04734	4	very weak
Bcc	002	~65 deg	1.43724	3	very weak
	112	~82 deg	1.17467	100	very strong
	013	~116 deg	0.90877	26.5	moderately strong
	222	~135.5 deg	0.83149	9.5	weak
DO_3	113	~53 deg	1.73592	58.8	strong
	226	~125 deg	0.8661	8	weak

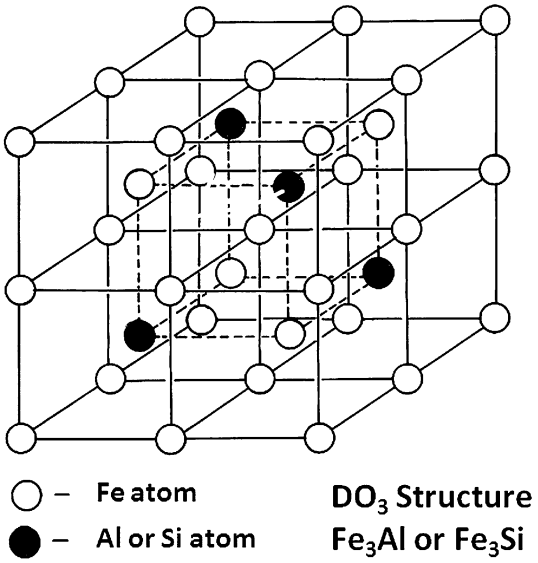

Fig. 15—Superlattice structure of DO_3 phase consisting of 8 bcc-type unit cells.

approximately 0.46 and 0.47, respectively, for Fe_3Al and Fe_3Si, which increased to about 0.87 and 0.88, respectively, after heat treatment. It may be noted that the order parameter did not change much with the heat-treatment temperature. This is possibly due to a disordering effect caused by the hot deformation, which resulted in lowering of order parameter in hot-rolled steel. Heavy deformation and heat treatment are known to cause huge impact on ordering of intermetallic phases. One such interesting example can be seen in a Ni_3Al-based duplex alloy.[17,18] In the present case, the order parameter increased again as soon as the material was subjected to heat treatment and remained almost constant thereafter. This observation clearly indicates that the so-called bcc ferrite phase of this steel is basically an ordered DO_3 phase. Moreover, the extent of ordering of this phase is also quite considerable.

In the described calculation, order parameter was measured on the basis of two hypothetical situations; either only aluminum was present, which combined with iron to form a DO_3 intermetallic compound, or only silicon was present, which combined with iron in a similar manner. However, it is also understood in the present case that the ordered DO_3 phase is neither pure Fe_3Al nor pure Fe_3Si, rather it would be justified to consider a combination of both intermetallic compounds. In that case, the value of order parameter would be different to some extent, because the total atomic fraction of aluminum and silicon would have to be considered. Since the atomic scattering factors of aluminum and silicon are very close,[16] considering a DO_3 phase of $Fe_3(Al,Si)$ type, the order parameter value would be about 10 pct higher than the values that were obtained considering only Fe_3Al or Fe_3Si (Figure 17). It is more important that the nature of changes in order parameter would still be exactly the same. The existence of DO_3 phase in Fe-Al-Si ternary system was also observed by Kozaki and Miyazaki,[19] who studied the 650 °C isotherm of Fe-Al-Si system. In the same article, they also reported the presence of DO_3 phase in a number of iron-base ternary alloys. As per their observation, the DO_3 phase field in 650 °C isotherm of Fe-Al-Si system was quite a large area. Considering the atomic fractions of aluminum and silicon in the present study, the formation of DO_3 phase in steel LC matches well with their report. However, the situation changed completely with increased carbon content as observed in steel HC and single-phase austenitic steel was obtained.

Another point that requires consideration is that the material contains a high percentage of manganese. Therefore, it is quite unlikely that the DO_3 phase is only constituted by Fe_3Al and Fe_3Si, rather it would be more realistic to consider the possibility of substitution of Fe atoms by Mn atoms in the superlattice structure and formation of intermetallic compounds of $(Fe,Mn)_3Al$ and $(Fe,Mn)_3Si$ type. The strong presence of manganese in bcc phase as obtained from EDS spectra of steel LC also supports this (Table V). Since the atomic scattering factors of iron and manganese are quite close,[16] there will be little effect of substitution of iron atoms by manganese atoms on the S parameter. Considering the XRD data of hot-rolled steel LC, the average lattice parameter of DO_3 phase was calculated to be 5.776 Å.

The significance of this observation has a direct relation with the mechanical property of steel LC. Ordered Fe_3Al- and Fe_3Si-based alloys with DO_3 structure are considered to be prospective structural intermetallics for high-temperature applications, due to their high-temperature strength and excellent creep

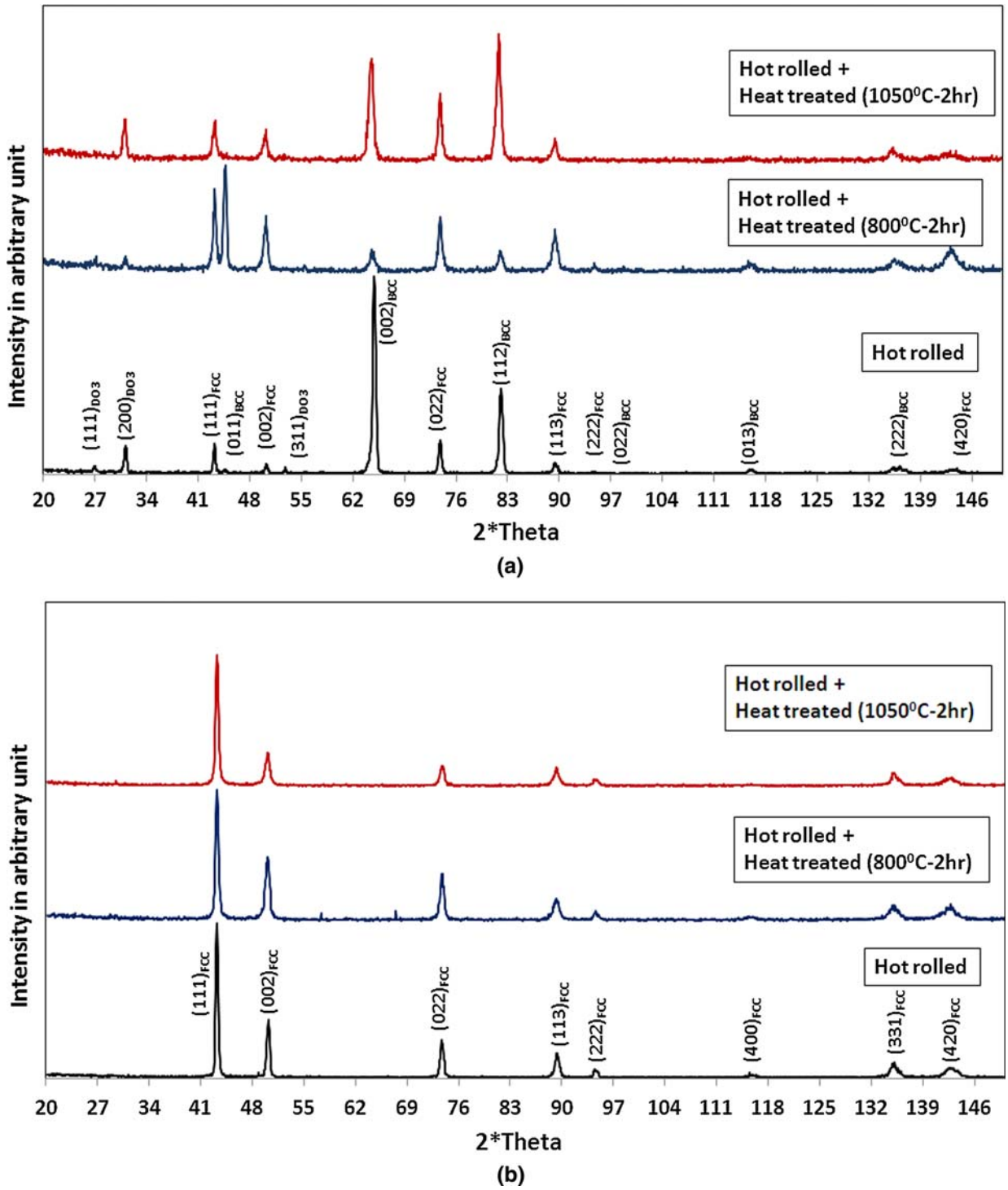

Fig. 16—(*a*) XRD profiles of steel LC at different conditions and (*b*) XRD profiles of steel HC at different conditions.

resistance. However, the ambient temperature ductility of these alloys is extremely poor.[20] A detailed study was carried out by McKamey *et al.*[21] on the mechanical properties of Fe_3Al alloys, which revealed that the tensile elongation of nearly stoichiometric Fe_3Al was almost close to zero. This observation is quite similar to the results of present investigation. The principal reason of poor ductility of this type of ordered alloys is associated with the superdislocations and antiphase domain boundaries. As a result, the fracture in room-temperature failure features transgranular-type cleavage facets, which are clearly visible in the micrographs shown in Figures 11(a) and (b). Transgranular cleavage fracture in Fe_3Si-based alloy has also been reported in

Table IV. (a) Indexing of XRD Profiles of Steel LC (Corresponding to Figure 16(a)). (b) Indexing of XRD Profiles of Steel HC (Corresponding to Figure 16(b))

Peak Positions	Reflecting Planes	d Spacing (Å)	Relative Intensity, I/I_{max} (Pct)		
			Hot Rolled	Hot Rolled + Heat Treated at 800 °C	Hot Rolled + Heat Treated at 1050 °C
(a)					
~26.5 deg	DO_3-111	3.35944	4.2	1.9	0
~31 deg	DO_3-200	2.87977	11.4	8.4	32.6
~53 deg	DO_3-311	1.73189	3.2	0	0.3
~43 deg	fcc-111	2.09881	13.6	71.6	28.9
~50 deg	fcc-200	1.81949	4.6	51.8	20.8
~73.5 deg	fcc-220	1.28578	13.4	46.2	49.7
~89.5 deg	fcc-311	1.0961	4.7	35.6	14.5
~94.5 deg	fcc-222	1.04737	0.4	0.7	0
~143 deg	fcc-420	0.81254	0.8	11.6	0.3
~44.5 deg	bcc-110	2.02996	0.3	100	0
~65 deg	bcc-200	1.44401	100	15.6	74
~82 deg	bcc-112	1.17584	41	17.3	100
~98.5 deg	bcc-220	1.01634	0	4.9	0
~116 deg	bcc-310*	0.91149	1.4	1.9	0.3
~135.5 deg	bcc-222*	0.83316	1.1	5.7	6.3
(b)					
~43 deg	fcc-111	2.09883	100	100	100
~50 deg	fcc-200	1.82469	34.6	47	24.3
~73.5 deg	fcc-220	1.28687	22.6	36.4	15.1
~89.5 deg	fcc-311	1.09791	14.9	15.6	13.8
~94.5 deg	fcc-222	1.04811	4.4	4.8	4.2
~116 deg	fcc-400	0.91001	0.1	1.4	0
~135 deg	fcc-331	0.83441	7	6.6	8.8
~143 deg	fcc-420	0.81345	2.2	3.9	2.8

*Note: fcc-400 and fcc-331 peaks, respectively, also appear at these locations. However, considering the weak intensities at these locations and also the weak presence of fcc phase in steel LC, the presence of fcc peaks at these two locations have been ignored.

Table V. Spot EDS Analysis of Bcc Phase in Steel LC

Conditions	Fe (At. Pct)	Mn (At. Pct)	Al (At. Pct)	Si (At. Pct)	Al + Si (At. Pct)
Hot rolled	56.43	26.27	8.04	9.26	17.30
Hot rolled + heat treated at 800 °C	56.66	21.95	10.56	10.82	21.38
Hot rolled + heat treated at 1050 °C	56.61	24.91	9.03	9.45	18.48

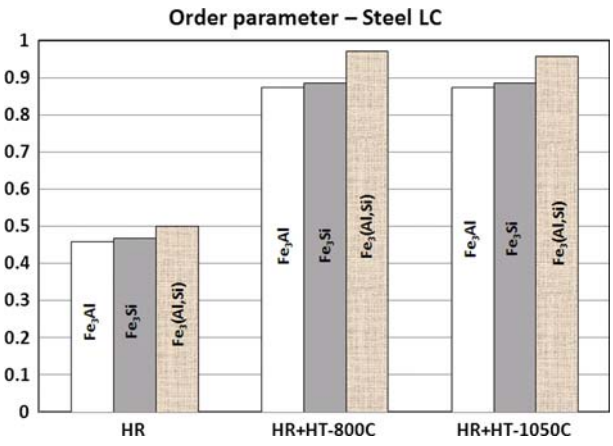

Fig. 17—Variation of order parameter for steel LC in three conditions.

literature.[22] The study of high-temperature ductility was not in the scope of present investigation, as the principal aim of this work was to explore the experimental alloys for the development of crash-resistant automobile components, which are likely to be used in ambient temperature.

Frommeyer and Brüx[23] also detected the presence of DO_3 phase in high-manganese steels, but their observation was different as far as the room temperature ductility is concerned. This is possibly because of the fact that they experimented with fairly high-carbon steels, which is an important factor for austenite stabilization. In fact, steel HC in the present investigation, with 0.5 pct C, has shown encouraging mechanical properties. Worldwide industrial development activities are also underway, based on the high-manganese steels with carbon content 0.5 pct or more.

IV. CONCLUSIONS

1. Twin-induced plasticity effect was obtained in steel HC, but steel LC showed no plasticity at all.
2. The ductility of steel LC was found to be extremely poor. This composition, both in hot-rolled and heat-treated conditions, failed under tensile loading at zero elongation.
3. Poor ductility of steel LC was due to the presence of an ordered DO_3 phase with a fairly high level of ordering. The magnitude of ordering increased when the hot-rolled steel was heat treated for 2 hours at two different temperatures, 800 °C and 1050 °C.
4. The superlattice structure of DO_3 phase was constituted of $(Fe,Mn)_3Al$ and $(Fe,Mn)_3Si$ type intermetallic compounds, with manganese atoms substituting iron atoms in the superlattice crystal structure.
5. Steel HC showed a combination of high strength and large tensile elongation. In hot-rolled condition the combination was 800 MPa UTS and 33 pct total elongation. The elongation further enhanced after heat treatment at 1050 °C for 2 hours, and the combination was 726 MPa UTS and 56 pct total elongation.
6. Larger grain size in heat-treated alloy (HC) resulted in higher tensile elongation, due to pronounced TWIP effect.

REFERENCES

1. S. Allain, J.-P. Chateau, and O. Bouaziz: *Mater. Sci. Eng. A*, 2004, vols. 387A–389A, pp. 143–47.
2. O. Grässel, L. Krüger, G. Frommeyer, and L.W. Meyer: *Int. J. Plast.*, 2000, vol. 16, pp. 1391–1409.
3. S. Vercammen, B. Blanpain, B.C. DeCooman, and P. Wollants: *Acta Mater*, 2004, vol. 52, pp. 2005–12.
4. Y.G. Kim, J.M. Han, and J.S. Lee: *Mater. Sci. Eng. A*, 1989, vol. 114, pp. 51–59.
5. N. Cabaňas, N. Akdut, J. Penning, and B.C. DeCooman: *Metall. Mater. Trans. A*, 2006, vol. 37A, pp. 3305–15.
6. P. Yang, Q. Xie, L. Meng, H. Ding, and Z. Tang: *Scripta Mater.*, 2006, vol. 55, pp. 629–31.
7. D. Hua, T.Z. You, L. Wei, W. Me, and S. Dan: *J. Iron Steel Res. Int.*, 2006, vol. 13 (6), pp. 66–70.
8. K. Ishida, H. Ohtani, N. Satoh, R. Kainuma, and T. Nishijawa: *ISIJ Int*, 1990, vol. 30, pp. 680–86.
9. O. Acselrad, I.S. Kalashnikov, E.M. Silva, R.A. Simao, C.A. Achete, and L.C. Pereira: *Metall. Mater. Trans. A*, 2002, vol. 33A, pp. 3569–73.
10. K. Sato, M. Ichinose, Y. Ohirotsu, and Y. Inoue: *ISIJ Int.*, 1989, vol. 29, pp. 868–77.
11. S. Allain, J.-P. Chateau, D. Dahmoun, and O. Bouaziz: *Mater. Sci. Eng.*, 2004, vols. A 387–A389, pp. 272–76.
12. D. Cornette, P. Cugy, A. Hildenbrand, M. Bouzekri, and G. Lovato: *Rev. Métallurgie-CIT*, 2005, Dec., pp. 905–18.
13. R. Ueji, K. Harada, N. Tsuchida, and K. Kunishige: *Mater. Sci. Forum*, 2007, vols. 561–565, pp. 107–10.
14. *ASM Handbook,* vol. 3, *Alloy Phase Diagrams*, ASM INTERNATIONAL, Metals Park, OH, 1992.
15. R. Ramesh, R. Vasudevan, B. Pathiraj, and B.H. Kolster: *J. Mater. Sci*, 1992, vol. 27, pp. 270–78.
16. B.D. Cullity: *Elements of X-Ray Diffraction*, Addison-Wesley, New York, NY, 1978.
17. B. Bhattacharya and R.K. Ray: *Metall. Mater. Trans. A*, 2000, vol. 31A, pp. 3001–10.
18. B. Bhattacharya and R.K. Ray: *Metall. Mater. Trans. A*, 2002, vol. 33A, pp. 3605–18.
19. T. Kozakai and T. Miyazaki: *ISIJ Int.*, 1994, vol. 34, pp. 373–83.
20. M.G. Mendiratta and H.A. Lips: in *High-Temperature Ordered Intermetallic Alloys*, C.C. Koch, C.T. Liu, and N.S. Stoloff, eds., MRS, Pittsburgh, PA, 1989, pp. 155–72.
21. C.G. McKamey, C.T. Liu, J.V. Cathcart, S.A. David, and E.H. Lee: *Evaluation of Mechanical and Metallurgical Properties of Fe_3Al Based Aluminides*, Oak Ridge National Laboratory, Oak Ridge, TN, 1986.
22. F. Sorbello, P.E.J. Flewitt, A.G. Crocker, and G.E. Smith: *Key Eng. Mater.*, 2008, vols. 385–87, pp. 1–4.
23. G. Frommeyer and U. Brüx: *Steel Res. Int.*, 2006, vol. 77, pp. 627–33.